The Mechanism of β-Hairpin Formation[†]

R. Brian Dyer,*[,‡] Shelia J. Maness,[§] Eric S. Peterson,[||] Stefan Franzen,[§] R. Matthew Fesinmeyer,[⊥] and Niels H. Andersen[⊥]

Bioscience Division, Mail Stop J586, Los Alamos National Laboratory, Los Alamos, New Mexico 87545, Chemistry Department, North Carolina State University, Raleigh, North Carolina 27695, Chemistry Department, Bowdoin College, Brunswick, Maine 04011, and Chemistry Department, University of Washington, Seattle, Washington 98195

Received April 23, 2004; Revised Manuscript Received July 2, 2004

ABSTRACT: β-Hairpins constitute an important class of connecting protein secondary structures. Several groups have postulated that such structures form early in the folding process and serve to nucleate the formation of extended β-sheet structures. Despite the importance of β-hairpins in protein folding, little is known about the mechanism of formation of these structures. While it is well established that there is a complex interplay between the stability of a β-hairpin and loop conformational propensity, loop length, and the formation of stabilizing cross-strand interactions (H-bonds and hydrophobic interactions), the influence of these factors on the folding rate is poorly understood. Peptide models provide a simple framework for exploring the molecular details of the formation of β-hairpin structures. We have explored the fundamental processes of folding in two linear peptides that form β-hairpin structures, having a stabilizing hydrophobic cluster connected by loops of differing lengths. This approach allows us to evaluate existing models of the mechanism of β-hairpin formation. We find a substantial acceleration of the folding rate when the connecting loop is made shorter (i.e., the hydrophobic cluster is moved closer to the turn). Analysis of the folding kinetics of these two peptides reveals that this acceleration is a direct consequence of the reduced entropic cost of the smaller loop search.

A fundamental process in protein folding is the formation of the secondary structural elements that compose the native structure. Peptide models have provided valuable experimental systems for studying the kinetics and mechanisms of secondary structure formation (*1*, *2*). Many related processes of protein folding have been observed in the folding of peptide models, including hydrophobic collapse, hydrogen bond formation, and side-chain packing (*3*−*6*). Studies of helical peptides have been particularly successful in elucidating the dynamics of helix nucleation and propagation and helix−helix interactions (*7*−*9*). Studies of the dynamics of β-structure formation have been more limited due to difficulties in designing suitable model systems. Some of the problems associated with β-sheet peptide models include their tendency to be large, prone to aggregate, not very stable, and low in secondary structure content. Consequently, the details of how β-structure forms as a protein folds remain elusive, despite the fundamental importance of these structures.

Advances have been made recently in the design of stable and soluble peptides with β-turn and β-sheet structures (*10*−*16*). Studies of these model systems are yielding clues about the molecular basis of stability of such structures. Furthermore, the dynamics of folding of a number of β-hairpin peptides have been reported recently, including the 16-residue C-terminal β-hairpin fragment of protein G [GB1 (*17*)], cyclic gramicidin analogues (*18*), and a de novo designed hairpin [HP1 (*19*)]. In all three cases, apparent two-state relaxation kinetics of the β-hairpin structure are observed using laser-induced temperature-jump (T-jump)[1] and time-resolved spectroscopic probes (Trp fluorescence or IR absorbance) of the folding reaction. Folding lifetimes at T_m for the noncyclic peptides derived from two-state kinetic models are 2.5 μs for GB1 and 0.7 μs for HP1. These lifetimes are substantially longer than the folding lifetimes of about 200 ns reported for similarly sized helical peptides under similar conditions (*8*, *9*). Muñoz et al. rationalize the slower rate within a kinetic zipper model by assuming that the hydrogen bond propagation rate is the same in both instances, which implies that the nucleation of a stable turn is much slower than helix nucleation. They postulate that hairpin nucleation is slow because it requires a cooperative stabilization by hydrophobic side-chain interactions. The observation of very fast folding ($\tau_f \sim 100$ ns) of "prenucleated" cyclic peptides that form a β-hairpin structure by our group provides support for this idea (*18*).

A number of theoretical approaches have been employed to model the folding mechanism of a β-hairpin, including Langevin simulations of minimal off-lattice models (*20*), all atom molecular dynamics (*21*), and multicanonical Monte Carlo simulations (*22*). A result common to all of these

[†] This research was supported by the National Institutes of Health, Grants GM53640 (R.B.D.) and GM59658 (N.H.A.).

* To whom correspondence should be addressed. Phone: (505) 667-4194. Fax: (505) 667-0851. E-mail: bdyer@lanl.gov.

[‡] Los Alamos National Laboratory.

[§] North Carolina State University.

[||] Bowdoin College.

[⊥] University of Washington.

[1] Abbreviations: T-jump, temperature jump; HC, hydrophobic cluster; FTIR, Fourier transform infrared; HFIP, hexafluoro-2-propanol; TFA, trifluoroacetate.

10.1021/bi049177m CCC: $27.50 © 2004 American Chemical Society
Published on Web 08/19/2004

studies is hairpin folding through discrete intermediates or through a hierarchy of structural changes involving hydrophobic collapse, hydrogen bond formation, and side-chain ordering. The model of Muñoz et al. suggests that folding nucleates at the turn, followed by sequential formation of cross-strand H-bonds increasingly remote from the turn locus (*23*). In this model, the hydrophobic core is formed after the turn and stabilizes the structure. In contrast, the simulations of Dinner et al. predict that hydrophobic collapse and rearrangement to produce a native-like topology are the key initial steps, followed by hydrogen bond formation. Thus, formation of a collapsed, native-like topology serves as a nucleating event, with hydrogen bonds propagating outward from the hydrophobic core. These models predict fundamentally different roles for the formation of the turn versus the hydrophobic core in the folding mechanism of the β-hairpin structure. In either case, hydrogen bond formation is seen as a fast propagation step that follows the nucleating event. Further work is clearly required to resolve these issues.

Our recent investigation of a series of cyclic β-hairpin peptides suggests that the collapse and topological search steps are rate limiting but that turn formation and hydrogen bond propagation in the collapsed chain are significantly faster, comparable to nucleation and propagation in helical peptides (*18*). Here we have explored these issues more directly using two noncyclic β-hairpin peptides, MrH3a (KKYTVSI**NG**KKITVSA) and BH8 (RGITV**NG**KTYGR). The turn sequence is highlighted in bold, and the residues which form the first cross-strand hydrophobic interactions are underlined. Both peptides form stable antiparallel β-hairpin structures, connected by a type I′ β-turn and are thus ideal systems in which to explore the dynamics and mechanism of β-hairpin formation. The MrH3a sequence is a modification (a C-terminal I to A substitution to improve solubility) of a previously reported sequence (*24*, *25*) designed to mimic the two-stranded, antiparallel β-sheet DNA-binding motif of the *met* repressor. BH8 is a de novo designed sequence first reported by the Serrano group (*26*) that places the hydrophobic "cluster" of the β-sheet closer to the turn region. We define the hydrophobic cluster (HC) as the region along the antiparallel sheet where the burial of hydrophobic surface area is maximized in the folded state. The interplay between the length and conformational propensity of the loop and hydrophobic cluster formation in influencing the stability of a β-hairpin is well established (*27*). Interestingly, the position of the hydrophobic cluster with respect to the turn has a marked effect on β-hairpin stability. In contrast, the effect of the position of the hydrophobic cluster on the rate of folding remains unknown, hence the importance of comparing the folding dynamics of the MrH3a and BH8 peptides. We find a significant acceleration of the folding rate occurs when the hydrophobic cluster is moved closer to the turn as a direct consequence of the reduced entropic cost of the smaller loop search.

MATERIALS AND METHODS

Peptides. Hairpin peptides were synthesized using FMOC chemistry on an Applied Biosystems 433A synthesizer. The C-terminal I to A substitution in MrH3a improves the peptide solubility and reduces its tendency to aggregate relative to the original sequence (*28*). Each peptide was purified by reverse-phase HPLC (C18 column) using a water/acetonitrile gradient and deuterium exchanged by repeated lyophilization from D_2O. Trifluoroacetic acid (TFA), which was used in the HPLC purification, was present as an impurity in all samples. Samples were dissolved in a solution of 21 vol % hexafluoro-2-propanol (HFIP) in D_2O (99.9%, Sigma) with no added buffer, and final concentrations were determined to be in the range of 1−4 mM as determined by the UV absorption of Tyr at 274 nm. The melting behavior of MrH3a and BH8 in water with and without added fluoro alcohol cosolvent has also been examined by NMR (*29*).

Infrared Spectroscopy. The equilibrium melting behavior of the hairpin peptides was studied using FTIR spectroscopy. FTIR spectra were collected on a Bio-Rad FTS-40 interferometer using a temperature-controlled IR cell. The IR cell contained both the sample and a D_2O reference solution between CaF_2 windows with a 100 μm spacer. The cell is translated laterally under computer control to acquire matching sample and reference single beam spectra, and the protein absorption spectrum is computed as $-\log(I_{samp}/I_{ref})$.

T-Jump Relaxation Measurements. The T-jump relaxation apparatus has been described previously (*9*). Briefly, a laser-induced T-jump is used to rapidly shift the folding/unfolding equilibrium, and the relaxation kinetics are measured using time-resolved infrared spectroscopy. The T-jump perturbation generated by a laser heating pulse is faster than the molecular dynamics of interest. The T-jump pulse is generated by Raman shifting a Q-switched Nd:YAG (Spectra Physics DCR-4) fundamental at 1064 nm in H_2 gas (1 Stokes shift), producing a 10 ns pulse at 1.91 μm. The near-infrared wavelength is partially absorbed by the D_2O ($\epsilon \sim 6$ cm^{-1}, or 87% transmittance in a 100 μm path length cell), and the absorbed energy is rapidly thermalized within the irradiated volume. The magnitude of the T-jump produced depends on the per pulse energy and the focus of the laser, typically 40 mJ and 1 mm spot diameter, respectively, which yields an 11 °C T-jump. The mid-IR probe beam is a continuous wave lead−salt diode laser (Laser Photonics) with a tunable output range of 1600−1700 cm^{-1}. The probe beam is focused to a 50 μm (1/e^2 diameter) spot at the center of the heated volume. Probing only the center of the heated volume ensures a uniform temperature distribution in the probe volume by avoiding the temperature gradient produced on the wings of the Gaussian pump beam (*30*). The transient transmission of the probe beam through the sample is measured using a fast (100 MHz) photovoltaic MCT IR detector/preamplifier (Kolmar Technologies). Transient signals are digitized and signal averaged using a Tektronics digitizer (7612D). Instrument control and data collection are accomplished using a LabVIEW computer program. Measurements of the transient absorbance for both the sample and the reference were collected from 10^{-9} to 10^{-1} s, and relaxation times were obtained using a deconvolution process described below.

Analysis of Kinetic Data. Accurate determination of the peptide relaxation kinetics requires deconvolution of the instrument response function from the observed kinetics. Very accurate deconvolution of the instrument response is possible because it is determined concurrently with each sample measurement under the exact same conditions. The instrument response function for the system is taken to be the derivative of the reference trace, normalized to have an integral of 1 at the maximum of the reference trace. The decay function used is an exponential decay with the formula

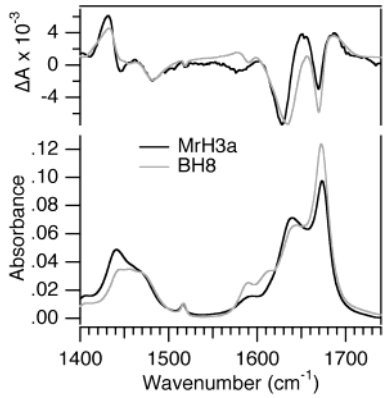

FIGURE 1: FTIR spectra of MrH3a and BH8 in the amide I and II spectral region obtained for 1 mM peptide in 21% (vol) HFIP in D_2O solution and an 83 μm cell path length. The spectra taken at 40 °C (MrH3a) and at 4 °C (BH8) were chosen for comparison because at these temperatures the peptides are mostly folded and the fraction folded is closely matched (each peptide is 70% folded at the respective temperatures). The peak at 1672 cm^{-1} is due to a TFA impurity present at slightly different concentrations in the two samples. The temperature-dependent difference spectra (40 − 10 °C) are compared in the offset to emphasize the spectral changes that accompany unfolding.

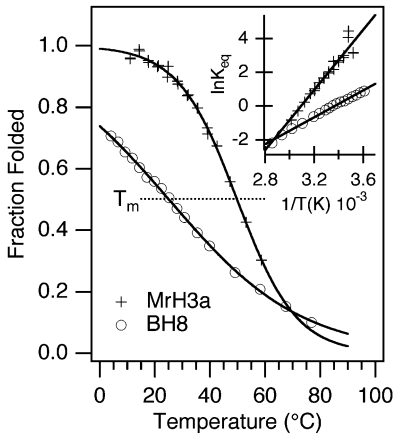

FIGURE 2: Comparison of the FTIR melts for MrH3a (+) and BH8 (○) in 21% (vol) HFIP in D_2O solution. The melt curves are determined by fitting the IR absorbance at 1636 cm^{-1} (the main β-sheet marker band) to a two-state model. The transition midpoints are indicated by the dotted line. Inset: van't Hoff analysis of the thermal transitions for MrH3a (+) and BH8 (○) under the same conditions.

[$A \exp(-kt)$], where A and k are the change in absorbance and the rate, respectively. The reported relaxation rates represent an average of at least four separate trials.

RESULTS

Equilibrium FTIR Studies. The spectroscopic evidence (CD, NMR, and IR) indicates that both peptides adopt β-hairpin (folded) structures in 21 vol % HFIP solution. In addition, the NMR evidence supports a cooperative two-state transition, with chemical shift melt profiles that are essentially identical for all of the proton resonances observed (*31*). The FTIR spectra of MrH3a and BH8 are compared in Figure 1. We focus on the amide I′ spectral region because this vibrational mode is an established indicator of secondary structure (*32*, *33*). This broad, multicomponent band contains contributions from the entire polypeptide backbone, which in this case adopts either a β-sheet, β-turn, or disordered conformation. The amide I′ maximum at room temperature is similar to that previously reported for other β-hairpin structures in D_2O, with a peak maximum at 1640 cm^{-1} (*34*, *35*). Most of the differences in the FTIR spectra of the two peptides are due to HOD and TFA impurities present at different concentrations (e.g., the sharp TFA peak centered at 1672 cm^{-1}). The second derivative spectra of both peptides show three amide I′ subcomponents at low temperatures (predominately folded conformation). These occur at 1628, 1634, and 1645 cm^{-1} for MrH3a and at 1629, 1637, and 1645 cm^{-1} for BH8. The slightly higher frequencies of the BH8 amide I′ modes are also evident in the position of the amide I′ absorbance maxima (Figure 1). We have demonstrated that these three components of amide I′ correspond to the β-turn and the inward and outward directed C═O groups of the β-sheet, i.e., intra- and intermolecular (to water) hydrogen bonding, respectively (*18*). The observation of these three components in the amide I′ band is clear evidence for the formation of a stable β-hairpin structure. In addition, the slightly higher frequencies observed for the intramolecular BH8 modes suggest that the net H-bonding is weaker in this case, consistent with the lower stability of the BH8 hairpin.

The difference spectra for each peptide, also shown in Figure 1, reveal the spectral changes that occur with temperature. These difference spectra are generated by subtraction of the lowest temperature spectrum of each peptide from the spectra at 40 °C. A bleach of the amide I′ mode is observed at 1630 cm^{-1} for MrH3a and at a slightly higher frequency for BH8, consistent with loss of the β-hairpin structure as temperature is increased. A single broad component centered at 1660 cm^{-1} grows in with increasing temperature (the notch in the middle of this band is the TFA impurity peak, which broadens with increasing temperature). The frequency and breadth of the 1660 cm^{-1} peak are essentially identical to what we have observed for both peptides and proteins and are characteristic of disordered polypeptide structure (*9*, *18*, *36*). The increase in frequency and bandwidth of the amide I′ mode upon unfolding is consistent with loss of strong intramolecular hydrogen bonding and an increase in inhomogeneity of the environment. The FTIR spectra therefore provide clear evidence for the loss of the folded conformation with increasing temperature.

Melting curves derived from the temperature-dependent FTIR spectra of both peptides are shown in Figure 2. The solid lines represent fits to a two-state model. MrH3a is clearly the more stable of the two peptides and shows a sharper melting transition. Thermodynamic parameters derived from a van't Hoff analysis (inset of Figure 2) are summarized in Table 1. The van't Hoff analysis is linear over a broad temperature range (70 °C), nearly spanning the transition in both cases, indicating that the heat capacity change ($\Delta C_p = d\Delta H/dT$) upon folding of each peptide is very small. This result is not surprising since the folded structure in both cases does not bury substantial hydrophobic surface area. This behavior is similar to that of HP1 (*19*) but contrasts with that of the Trpzip sequences (*15*), which have a large hydrophobic cluster formed by four Trp side chains and, consequently, exhibit a large ΔC_p of folding (~300 cal K^{-1} mol^{-1}). Thermodynamic parameters for three related β-hairpin peptides are also given in Table 1. The stability of BH8 is similar to HP1 and to the stability reported

Table 1: Thermodynamic and Kinetic Parameters for β-Hairpin Folding

peptide	T_m/ °C	ΔH_f/ kJ mol^{-1}	ΔS_f/ J mol^{-1} K^{-1}	N	k_r^a/s^{-1}
cyclic 14-mer[b]	71	-48.3 ± 0.5	-140 ± 2	2	9.1×10^6
BH8 (21% HFIP)	25	-33.1 ± 0.6	-111 ± 2	5	1.9×10^6
HP1[c]	29	-28	-92	6	1.4×10^6
MrH3a (21% HFIP)	50	-74 ± 4	-229 ± 15	9	4.3×10^5
GB1[d]	24	-48.5	-163	9	4.0×10^5

[a] Relaxation rate determined at the midpoint (T_m). [b] From ref *18*. [c] From ref *19*. [d] From ref *17*.

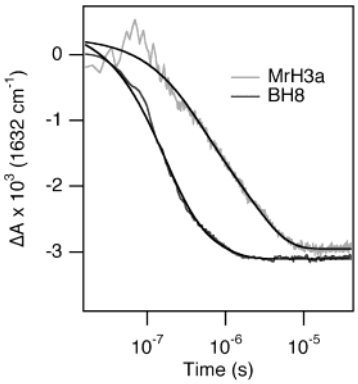

FIGURE 3: Relaxation kinetics of MrH3a and BH8 in 21% (vol) HFIP in D_2O following a laser-induced T-jump. The kinetics are monitored at 1632 cm^{-1}, near the peak of the main β-hairpin marker band. The T-jumps are close to the transition midpoints in each case ($\Delta T = 40-46$ °C for MrH3a and $20-24$ °C for BH8). The absorbance change is negative, consistent with shifting the equilibrium toward a more unfolded position. The data were fitted using a single exponential decay function convolved with the instrument response (see Materials and Methods). The amplitude of the single exponential phase matches the amplitude of the equilibrium difference between the starting and ending temperatures determined in FTIR measurements.

by Munoz et al. for GB1 but much less than that of MrH3a. It should be noted, however, that other experimental measurements of GB1 stability find that it is substantially less stable (only 42% folded at 5 °C) (*15*, *31*).

Temperature-Jump Relaxation Kinetics. The relaxation kinetics following a laser induced T-jump were probed using time-resolved infrared spectroscopy in the amide I′ band. Figure 3 displays the relaxation kinetics for both peptides following a small (3−5 °C) laser-induced T-jump. In both cases the T-jump is close to the midpoint of the transition (T_m is 25 °C for BH8 and 50 °C for MrH3a, as shown by the dashed line in Figure 2). This allows direct comparison of the relaxation rates at the same stability point, where the barrier height is simply the activation energy. The BH8 relaxation rate is clearly significantly greater (~4×) than that of MrH3a.

The data are well fit by a single exponential decay in each case. The early time region (~10^{-7} s) has a small cavitation artifact that is particularly evident in the MrH3a data. This artifact appears in the reference data (D_2O solutions that do not contain peptide) and has a characteristic time response and variable amplitude. We have selected kinetic traces for which it is small (<5% of the total signal amplitude) to minimize the effect on the kinetic fits. All of the relaxation kinetics observed for these peptides are single exponentials, regardless of starting temperature or magnitude of the T-jump. Furthermore, the equilibrium changes in the FTIR

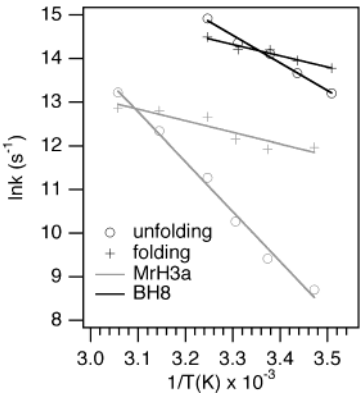

FIGURE 4: Arrhenius analysis of the temperature-dependent folding (+) and unfolding (○) rates of MrH3a (light) and BH8 (dark). Folding and unfolding rates were determined using a two-state analysis and equilibrium constants determined from the FTIR melt curves.

and NMR spectra as a function of temperature are best modeled in terms of two states (folded and unfolded structures) as discussed above. We have therefore analyzed the relaxation kinetics using a two-state model, for which the observed relaxation rate is the sum of the folding and unfolding rates, and the equilibrium constant is the ratio of these rates. The folding rates determined at the reaction midpoint are summarized in Table 1, along with those for the GB1 (*17*), HP1 (*19*), and cyclic 14-mer β-hairpin structures (*18*). The loop length, N, defined as the number of peptide bonds in the loop connecting the residues that form the first cross-strand, stabilizing interaction in the hydrophobic cluster, is also listed for each peptide.

Arrhenius plots of the temperature-dependent folding and unfolding rates of MrH3a and BH8 are shown in Figure 4. Folding and unfolding rates were determined using a two-state analysis of the relaxation rate, k_r ($k_r = k_f + k_u$), and equilibrium constants determined from the FTIR melt curves of Figure 2 ($K_{eq} = k_f/k_u$). We also assume that the activation parameters are temperature independent for this analysis. While other hairpins show a nonzero ΔC_p term for folding in water (probably due to burial of hydrophobic side chains), we have found that ΔC_p becomes very small when the fluoro alcohol concentration exceeds 16% v/v (*25*), which justifies this assumption. It is also clear that both the folding and unfolding Arrhenius plots in Figure 4 are linear within experimental error, consistent with a small ΔC_p term. The folding activation energies derived from the linear fits for both MrH3a and BH8 are the same, $E_a = 22$ kJ mol^{-1}. The rate of folding of the GB1 hairpin has been shown to be inversely proportional to the solvent viscosity, $k_f = k_0/\eta \exp(-\Delta G/RT)$ (*37*). Assuming a similar viscosity dependence for the MrH3a and BH8 structures, the temperature dependence of the viscosity of D_2O introduces a correction of 15 kJ mol^{-1}, yielding an enthalpy of activation ($\Delta H_f^{\ddagger}$) of 7 kJ mol^{-1} for each peptide. This small enthalpic barrier is similar to that observed for GB1 and HP1. There is also an entropic contribution to the folding barrier, but determination of the activation entropy requires a value for the preexponential factor. A recent study of the end-to-end contact rates in polypeptides found a limiting rate for minimum loop formation (i.e., formation of i, $i + 3$ interactions) of 2×10^8 s^{-1} (*38*). Krieger et al. postulate that this rate is a fundamental property of polypeptide chains and represents

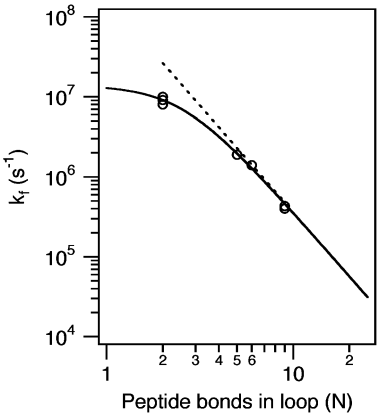

FIGURE 5: Effect of loop length, N (defined in text), on folding rate. The circles represent the data from Table 1. The solid line is a fit to the equation $k_f = 1/(1/k_0 + 1/k_i N^m)$, where $k_0 = 10^7$ s^{-1} and $m = -2.6$. The dashed line shows the length dependence for longer loop scales as $N^{-2.6}$.

a reasonable preexponential factor for protein folding reactions. Using 2×10^8 s^{-1} as the preexponential factor, we calculate $\Delta S_f^{\ddagger} = -28$ J mol^{-1} K^{-1} for MrH3a and $\Delta S_f^{\ddagger} = -14$ J mol^{-1} K^{-1} for BH8. Regardless of the absolute value of the preexponential factor (and hence of $\Delta S_f^{\ddagger}$), the origin of the difference between the folding rates of MrH3a and BH8 is clearly revealed by the Arrhenius analysis of Figure 4. The slopes corresponding to the folding rates for MrH3 and BH8 are nearly identical (enthalpic contribution to the folding barrier) whereas the intercepts are quite different (entropic contribution).

The dependence of the folding rate on the loop length, N, is analyzed in Figure 5. The data are for all known folding rates of β-hairpin structures, summarized in Table 1. The fit is to the equation $k_f = 1/(1/k_0 + 1/k_i N^m)$, analogous to the model used to analyze the rate of end-to-end contact formation in polypeptide chains (*38*). The folding rate clearly reaches a limiting value of about 10^7 s^{-1} for small loop searches ($N < 5$). For longer loop searches, the rate scales as $N^{-2.6\pm0.4}$. The uncertainty of the exponent is from the fit and is due to the limited range of loop lengths for which data are currently available.

DISCUSSION

β-Hairpins constitute an important class of connecting protein secondary structures. Several groups have postulated that such structures form early in the folding process and serve to nucleate the formation of extended β-sheet structures (*39*−*42*). Despite the importance of β-hairpins in protein folding, little is known about the mechanism of formation of these structures. It is well established (*27*) that there is a complex interplay between the stability of a β-hairpin and a number of factors, including the loop conformational propensity, the loop length, and the formation of stabilizing cross-strand interactions (H-bonds and hydrophobic interactions). The influence of these factors on the folding rate, however, is poorly understood. Peptide models provide a simple framework for exploring the molecular details of the formation of β-hairpin structures. We have explored the fundamental processes of the folding of two linear peptides that form β-hairpin structures, having a stabilizing hydrophobic cluster at different distances from the turn. The results reveal a strong dependence of the folding rate on the length of the loop connecting the stabilizing, cross-strand interactions of the hydrophobic cluster.

The folding rates of BH8 and MrH3a at the transition midpoint are compared in Table 1. Comparison of these rates at the transition midpoint compensates for the differing stabilities of the hairpin structures for each of these peptides. The location of the hydrophobic cluster relative to the turn region is two residues closer to the turn for BH8 compared to MrH3a. Consequently, the loop connecting the first residues which form the stabilizing, cross-strand interactions are five and nine residues apart, respectively. The folding rate of BH8 is significantly faster than that of MrH3a. If the activation barriers were the same for BH8 and MrH3a, the rate for MrH3a would be 2.5 times faster based on the difference in T_m between the two peptides. The opposite trend is observed since the rate for BH8 is 4 times faster than that of MrH3a. The difference in rates is due to the difference in the activation barriers for the two peptides. Furthermore, the Arrhenius analysis of Figure 4 clearly indicates that the difference in barrier heights is due to the entropic contribution. The difference in barrier heights at the transition midpoints is thus $T_m \Delta S_{f\,BH8}^{\ddagger} - T_m \Delta S_{f\,MrH3a}^{\ddagger} = 4.9$ kJ mol^{-1}, or about $2kT$.

We have tested the generality of these observations by comparing the rates of β-hairpin formation for MrH3a and BH8 with other model systems. Thus, for GB1 with $N = 9$, the folding rate is nearly identical to MrH3a, whereas HP1 with $N = 6$ has a folding rate intermediate to that of MrH3a and BH8. The dependence of the folding rate on loop length follows the same functional form as that used to describe the rate of end-to-end contact formation in polypeptide chains (*38*). Figure 5 shows that the folding rate has two different regimes: at short loop lengths, it approaches a limiting value of 10^7 s^{-1}, whereas at long loop lengths, it scales as $N^{-2.6\pm0.4}$. This result indicates that entropy-controlled intrachain diffusion is a key determinant of the folding rate. Analogous to chain diffusion, the breakdown of the scaling law at short loop lengths is likely due to the effect of chain stiffness (*43*). Two important differences are evident in the behavior of β-hairpin formation compared to simple polypeptide chain diffusion. First, the breakpoint (below which the rate no longer follows the power law dependence on loop length) occurs near $N < 5$, at a much smaller distance than predicted by the Flory model ($N < 10$) and than actually observed for end-to-end contact rates in polypeptides [e.g., for poly(GlySer), $N < 20$]. Thus the loop appears to be less stiff than predicted, possibly because of the presence of the turn sequence in the middle of the loop. Furthermore, the length dependence for longer loops is clearly stronger than that expected for an entropy-controlled intrachain diffusion of an ideal Gaussian chain ($N^{-1.5}$) (*44*), even when corrected for excluded volume effects ($N^{-1.8}$) (*38*). This stronger dependence of the rate on loop length represents an additional barrier to folding, most likely due to a requirement for multiple contacts to form a stable interaction.

Comparison of the rate of β-hairpin formation to the rate of chain collapse provides additional evidence for the importance of stabilization of the collapsed polypeptide chain. The time required for the collapse of a polypeptide chain to form a loop of length N has been characterized by several groups (*38*, *45*, *46*) and ranges from 10^7 to 10^8 s^{-1}

for the loop lengths in the β-hairpins we have studied. This range of rates provides an upper limit for the rate at which the β-hairpin sequences sample compact conformations. The folding rate of each of the linear peptides is much slower, however, indicating either that the residence times in compact conformations are small until specific stabilizing interactions are made or that collapsed structures are quickly stabilized but with the wrong registry and must rearrange over a barrier to reach the correct fold.

Further insight on the loop search process is provided by our work on a series of cyclic peptides that form stable β-hairpin structures (*18*). The folding rates for the three different cyclic peptides examined are all about 10^7 s^{-1} (the data for the 6-mer and 10-mer are included in Figure 5 but not shown in Table 1). The critical loop size is constant across the series despite the range in size of the peptides and is likely defined by the formation of the i, $i + 3$ interactions in the hairpin turn ($N = 2$). In essence, the folding rate of the cyclic peptides represents the upper limit for β-hairpin formation because of the minimal loop search required. The cyclic structures are obviously constrained from sampling extended conformations, which likely causes an additional increase in the folding rate. A similar result has been observed in the folding of src SH3, for which the rate-limiting step in folding involves the formation of a β-hairpin structure. Insertion of a disulfide cross-link at the base of the distal β-hairpin in src SH3 increases the rate of folding of this protein 30-fold (*47*). This result has been interpreted as evidence for the formation of the hairpin structure in the transition state and a reduction in the transition state barrier (corresponding to the loop entropy) caused by formation of the disulfide linkage. Two recent theoretical simulations from the Thirumalai group support these ideas. First, Klimov and Thirumalai compared the rate of folding of a 16-residue, linear peptide with the cyclic analogue (formed by cross-linking the C and N termini) and found a 2.5 times acceleration for the cyclic peptide (*43*). Second, Klimov et al. found a greater than 2-fold increase in the rate of folding of the β-haipin from Ig-binding protein when confined in an inert spherical pore (*48*).

Two different models have been proposed for the mechanism of β-hairpin formation in the GB1 peptide, neither of which is fully consistent with our results. The first is the statistical mechanical model of Muñoz et al. (*17*, *23*), which postulates that the turn formation is the first step in folding followed by the zipping of the strands. The Muñoz model predicts that a large part of the transition state barrier is entropic; that is, the formation of the turn and initial zipping involves a loss of configurational entropy that is not compensated by the enthalpy gained by forming H-bonds. In this model, the turn is not stabilized until the first stabilizing hydrophobic interactions are formed. The turn forms rapidly but can dissolve many times before the peptide zips up. A contrasting model has been developed by Dinner et al., based on simulation of the equilibrium free energy profiles (*22*). The key prediction of the Dinner model is that the initial folding step is a nonspecific hydrophobic collapse. In this model, the transition barrier is primarily due to the energetic cost of interconverting compact forms to find the native alignment of the residues that form the hydrophobic cluster.

Muñoz et al. simulated the effect of moving the hydrophobic cluster closer to the turn in GB1 and found a dramatic perturbation of the free energy profile. The free energy of the folded ensemble and the top of the barrier are both reduced in the simulation, resulting in an increase in stability and an acceleration of the folding rate. If the cluster is moved further from the turn, the opposite effect on the stability and folding rate is observed. This result has been called into question, however, by the simulations of Dinner et al. (*22*), which show that the barrier in the Muñoz model disappears when structures containing more than one segment of native peptide bonds are considered. According to Dinner et al., this barrier is an artifact of the single sequence approximation (and its modifications), which only considers those structures with a single segment of native peptide bonds. Furthermore, the model of Muñoz et al. predicts a negative enthalpy of activation due to the formation of the native stabilizing cross-strand interactions in the transition state, whereas we actually observe a positive activation enthalpy for both MrH3a and BH8. While the observed $\Delta H_f^{\ddagger}$ is small, it is definitely positive (Figure 4), meaning that for MrH3a and BH8 (in contrast to GB1) enthalpy input is required to reach the transition state. It is possible that the relative contributions of enthalpic and entropic effects to the transition state barrier vary with turn structure and thus may be different for the six-residue turns found in GB1 analogues.

The simulations of Dinner et al. did not specifically test the effect of the position of the HC on the folding mechanism. The rate of initial collapse should depend on the length of the loop connecting the hydrophobic residues, as we have already discussed. It seems unlikely, however, that the rearrangement of collapsed conformations over a barrier (i.e., breaking non-native interactions) to form the native inter-strand registry and hence the stabilizing native interactions should have any dependence on the location of the hydrophobic cluster with respect to the turn.

The efficiency of the loop search is clearly related to the position of the stabilizing hydrophobic cluster relative to the turn region. Our results support a model for β-hairpin folding in which the rate-limiting step is the loop search process, which involves both an entropic barrier due to the loss of entropy caused by loop formation and an enthalpic barrier, which could be due to rearrangement of the collapsed structures. The latter is analogous to the barrier observed in the simulations of Dinner et al. due to the initial formation of non-native interactions which must be broken to form the correct ones. The enthalpic barrier is the same height for MrH3a and BH8, consistent with the nearly identical composition of the hydrophobic clusters in the two peptides. The size of the entropic barrier is different, however, and clearly related to the loop length. Placing the hydrophobic cluster adjacent to the turn in BH8 minimizes the loop length and accelerates the folding rate close to the speed limit established by the cyclic hairpin models.

REFERENCES

1. Callender, R. H., Dyer, R. B., Gilmanshin, R., and Woodruff, W. H. (1998) Fast Events in Protein Folding: The Time Evolution of Primary Processes, *Annu. Rev. Phys. Chem. 49*, 173−202.
2. Eaton, W. A., Munoz, V., Hagan, S. J., Jas, G. S., Lapidus, L. J., Henry, E. R., and Hofrichter, J. (2000) Fast Kinetics and Mechanisms in Protein Folding, *Annu. Rev. Biophys. Biomol. Struct. 29*, 327−359.

3. Espinosa, J. F., and Gellman, S. H. (2000) A Designed beta-Hairpin Containing a Natural Hydrophobic Cluster, *Angew. Chem., Int. Ed. 39*, 2330−2333.
4. Krantz, B. A., Moran, L. B., Kentsis, A., and Sosnick, T. R. (2000) D/H amide kinetic isotope effects reveal when hydrogen bonds form during protein folding, *Nat. Struct. Biol. 7*, 62−71.
5. Ramirez-Alvarado, M., Kortemme, T., Blanco, F. J., and Serrano, L. (1999) beta-Hairpin and beta-Sheet Formation in Designed Linear Peptides, *Bioorg. Med. Chem. 7*, 93−103.
6. Syud, F. A., Stanger, H. E., and Gellman, S. H. (2001) Interstrand Side Chain−Side Chain Interactions in a Designed β-Hairpin: Significance of Both Lateral and Diagonal Pairings, *J. Am. Chem. Soc. 123*, 8667−8677.
7. Dyer, R. B., Gai, F., Woodruff, W. H., Gilmanshin, R., and Callender, R. H. (1998) Infrared Studies of Fast Events in Protein Folding, *Acc. Chem. Res. 31*, 709−716.
8. Werner, J. H., Dyer, R. B., Fesinmeyer, R. M., and Andersen, N. H. (2002) Dynamics of the Primary processes of protein folding: Helix nucleation, *J. Phys. Chem. B 106*, 487−494.
9. Williams, S., Causgrove, T. P., Gilmanshin, R., Fang, K. S., Callender, R. H., Woodruff, W. H., and Dyer, R. B. (1996) Fast Events in Protein Folding: Helix Melting and Formation in a Small Peptide, *Biochemistry 35*, 691−697.
10. Smith, C. K., and Regan, L. (1997) Construction and Design of β-Sheets, *Acc. Chem. Res. 30*, 153−161.
11. Gellman, S. H. (1998) Minimal model systems for beta sheet secondary structure in proteins, *Curr. Opin. Chem. Biol. 2*, 717−725.
12. Schenck, H. L., and Gellman, S. H. (1998) Use of a Designed Triple-Stranded Antiparallel β-Sheet to Probe β-Sheet Cooperativity in Aqueous Solution, *J. Am. Chem. Soc. 120*, 4869−4870.
13. Griffiths-Jones, S. R., Maynard, A. J., and Searle, M. S. (1999) Dissecting the Stability of a β-Hairpin Peptide that Folds in Water, *J. Mol. Biol. 292*, 1051−1069.
14. Jäger, M., Nguyen, H., Crane, J. C., Kelly, J. W., and Gruebele, M. (2001) The Folding Mechanism of a β-Sheet: The WW Domain, *J. Mol. Biol. 311*, 373−393.
15. Cochran, A. G., Skelton, N. J., and Starovasnik, M. A. (2001) Tryptophan zippers: Stable, monomeric β-hairpins, *Proc. Natl. Acad. Sci. U.S.A. 98*, 5578−5583.
16. Searle, M. S. (2001) Peptide Models of Protein Beta-Sheets: Design, Folding and Insights into Stabilising Weak Interactions, *J. Chem. Soc., Perkin Trans. 2*, 1011−1020.
17. Muñoz, V., Thompson, P. A., Hofrichter, J., and Eaton, W. A. (1997) Folding dynamics and mechanism of β-hairpin formation, *Nature 390*, 196−199.
18. Maness, S. J., Franzen, S., Gibbs, A. C., Causgrove, T. P., and Dyer, R. B. (2003) Nanosecond Temperature Jump Relaxation Dynamics of Cyclic β-Hairpin Peptides, *Biophys. J. 84*, 3874−3882.
19. Xu, Y., Oyola, R., and Gai, F. (2003) Infrared Study of the Stability and Folding Kinetics of a 15-Residue β-Hairpin, *J. Am. Chem. Soc. 125*, 15388−15394.
20. Klimov, D. K., and Thirumalai, D. (2000) Mechanisms and Kinetics of β-Hairpin Formation, *Proc. Natl. Acad. Sci. U.S.A. 97*, 2544−2549.
21. Pande, V. S., and Rokhsar, D. S. (1999) Molecular Dynamics Simulations of Unfolding and Refolding of a b-hairpin Fragment of Protein G, *Proc. Natl. Acad. Sci. U.S.A. 96*, 9062−9067.
22. Dinner, A., Lazaridis, T., and Karplus, M. (1999) Understanding β-Hairpin Formation, *Proc. Natl. Acad. Sci. U.S.A. 96*, 9068−9073.
23. Muñoz, V., Henry, E. R., Hofrichter, J., and Eaton, W. A. (1998) A Statistical Mechanical Model for β-Hairpin Kinetics, *Proc. Natl. Acad. Sci. U.S.A. 95*, 5872−5879.
24. Maynard, A. J., Sharman, G. J., and Searle, M. S. (1998) Origin of β-Hairpin Stability in Solution: Structural and Thermodynamic Analysis of the Folding of a Model Peptide Supports Hydrophobic Stabilization in Water, *J. Am. Chem. Soc. 120*, 1996−2007.
25. Andersen, N. H., Dyer, R. B., Fesinmeyer, R. M., Gai, F., Liu, Z. H., Neidigh, J. W., and Tong, H. (1999) Effect of hexafluoroisopropanol on the thermodynamics of peptide secondary structure formation, *J. Am. Chem. Soc. 121*, 9879−9880.
26. Ramirez-Alvarado, M., Blanco, F. J., and Serrano, L. (1996) De Novo Design and Structural Analysis of a Model β-Hairpin Peptide System, *Nat. Struct. Biol. 3*, 604−612.
27. Espinosa, J. F., Munoz, V., and Gellman, S. H. (2001) Interplay between Hydrophobic Cluster and Loop Propensity in β-Hairpin Formation, *J. Mol. Biol. 306*, 397−402.
28. Colley, C. S., Griffiths-Jones, S. R., George, M. W., and Searle, M. S. (2000) Do Interstrand Hydrogen Bonds Contribute to β-Hairpin Peptide Stability in Solution? IR Analysis of Peptide Folding in Water, *Chem. Commun. 2000*, 593−594.
29. Andersen, N. H., Dyer, R. B., Fesinmeyer, R. M., Matthew, R., Gai, F., Maness, S. J., and Werner, J. H. (2001) in *Peptides 2000* (Martinez, J., and Fehrentz, J.-A., Eds.) pp 553−554, EDK, Paris, France.
30. Wray, W. O., Aida, T., and Dyer, R. B. (2002) Photoacoustic Cavitation and Heat Transfer Effects in the Laser-Induced Temperature Jump in Water, *Appl. Phys. B 74*, 57−66.
31. Fesinmeyer, R. M., Hudson, F. M., and Andersen, N. H. (2004) Enhanced Hairpin Stability through Loop Design: The Case of the Protein GB1 Hairpin, *J. Am. Chem. Soc. 126*, 7238−7243.
32. Arrondo, J. L. R., Blanco, F. J., Serrano, L., and Goni, F. M. (1996) Infrared Evidence of a β-Hairpin Peptide Structure in Solution, *FEBS Lett. 384*, 35−37.
33. Susi, H., and Byler, D. M. (1986) Resolution Enhanced Fourier Transform Infrared Spectroscopy of Enzymes, *Methods Enzymol. 130*, 290−311.
34. Lewis, R. N. A. H., Prenner, E. J., Kondejewski, L. H., Flach, C. R., Mendelsohn, R., Hodges, R. S., and McElhaney, R. N. (1999) Fourier Transform Infrared Spectroscopic Studies of the Interaction of the Antimicrobial Peptide Gramicidin S with Lipid Micelles and with Lipid Monolayer and Bilayer Membranes, *Biochemistry 38*, 15193−15203.
35. Tatulian, S. A., Jones, L. R., Reddy, L. G., Stokes, D. L., and Tamm, L. K. (1995) Secondary Structure and Orientation of Phopholamban Reconstituted in Supported Bilayers from Polarized Attenuated Total Reflection FTIR Spectroscopy, *Biochemistry 34*, 4448−4456.
36. Gilmanshin, R., Williams, S., Callender, R. H., Woodruff, W. H., and Dyer, R. B. (1997) Fast events in protein folding: Relaxation dynamics of secondary and tertiary structure in native apomyglobin, *Proc. Natl. Acad. Sci. U.S.A. 94*, 3709−3713.
37. Jas, G. S., Eaton, W. A., and Hofrichter, J. (2001) Effect of Viscosity on the Kinetics of α-Helix and β-Hairpin Formation, *J. Phys. Chem. B 105*, 261−272.
38. Krieger, F., Fierz, B., Bieri, O., Drewello, M., and Kiefhaber, T. (2003) Dynamics of Unfolded Polypeptide Chains as Model for the Earliest Steps in Protein Folding, *J. Mol. Biol. 332*, 265−274.
39. Grantcharova, V. P., Riddle, D. S., Santiago, J. V., and Baker, D. (1998) Important Role of Hydrogen Bonds in the Structurally Polarized Transition State for Folding of the src SH3 Domain, *Nat. Struct. Biol. 5*, 714−720.
40. Kortemme, T., Kelly, M. J. S., Kay, L. E., Forman-Kay, J., and Serrano, L. (2000) Similarities between the Spectrin SH3 Domain Denatured State and Its Folding Transition State, *J. Mol. Biol. 297*, 1217−1229.
41. Matheson, R. R., Jr., and Scheraga, H. A. (1978) A Method for Predicting Nucleation Sites for Protein Folding Based on Hydrophobic Contacts, *Macromolecules 11*, 819−829.
42. McCallister, E. L., Alm, E., and Baker, D. (2000) Critical Role of β-Hairpin Formation in Protein G Folding, *Nat. Struct. Biol. 7*, 669−673.
43. Klimov, D. K., and Thirumalai, D. (2002) Stiffness of the Distal Loop Restricts the Structural Heterogeneity of the Transition State Ensemble in SH3 Domains, *J. Mol. Biol. 315*, 721−737.
44. Szabo, A., Schulten, K., and Schulten, Z. (1980) First Passage Time Approach to Diffusion Controlled Reactions, *J. Chem. Phys. 72*, 4350−4357.
45. Bieri, O., Wirz, J., Hellrung, B., Schutkowski, M., Drewello, M., and Kiefhaber, T. (1999) The Speed Limit for Protein Folding Measured by Triplet−Triplet Energy Transfer, *Proc. Natl. Acad. Sci. U.S.A. 96*, 9597−9601.
46. Lapidus, L. J., Eaton, W. A., and Hofrichter, J. (2000) Measuring the Rate of Intramolecular Contact Formation in Polypeptides, *Proc. Natl. Acad. Sci. U.S.A. 97*, 7220−7225.
47. Grantcharova, V. P., Riddle, D. S., and Baker, D. (2000) Long-Range Order in the src SH3 Folding Transition State, *Proc. Natl. Acad. Sci. U.S.A. 97*, 7084−7089.
48. Klimov, D. K., Newfield, D., and Thirumalai, D. (2002) Simulations of β-Hairpin Folding Confined to Spherical Pores Using Distributed Computing, *Proc. Natl. Acad. Sci. U.S.A. 99*, 8019−8024.

BI049177M